MNRAS **000**, 1-10 (2015) Preprint 12 July 2015 Compiled using MNRAS LATEX style file v3.0

The Carnegie RR Lyrae Program: The Mid–Infrared RR Lyrae Period–Luminosity Relation in ω Cen

Meredith J. Durbin[1,2]⋆ Victoria Scowcroft[3] Wendy Freedman[4] Gurtina Besla[5] Giuseppe Bono[6,7] Maria–Rosa Cioni[8,9,10] Gisella Clementini[11] Kathryn Johnston[12] Nitya Kallivayalil[13] Juna Kollmeier[3] David Law[2] Barry Madore[3] Steve Majewski[13] Roeland van der Marel[2] Massimo Marengo[14] Andrew J. Monson[3] David Nidever[15] Grzegorz Pietrzynski[16,17] George Preston[3] Mark Seibert[3] Horace Smith[18] Igor Soszynski[16] Ian Thompson[3] Andrzej Udalski[16]

[1] *Pomona College, Claremont, CA 91711, USA*
[2] *Space Telescope Science Institute, 3700 San Martin Drive, Baltimore, MD 21218, USA*
[3] *Observatories of the Carnegie Institution of Washington, 813 Santa Barbara St., Pasadena, CA 91101, USA*
[4] *Department of Astronomy and Astrophysics, University of Chicago, 5640 S Ellis Ave, Chicago, IL 60637, USA*
[5] *Department of Astronomy and Steward Observatory, University of Arizona, 933 North Cherry Avenue, Tucson, AZ 85721, USA*
[6] *Univ. Roma "Tor Vergata", Via della Ricerca Scientifica, 1 - 00133, Roma, Italy*
[7] *INAF-OAR, via Frascati 33 - 00040, Monte Porzio Catone (RM), Italy*
[8] *Universtat Potsdam, Institut fur Physik und Astronomie, Karl-Liebknecht-Str. 24/25, 14476 Potsdam, Germany*
[9] *Leibniz-Institut fur Astrophysik Potsdam, An der Sternwarte 16, 14482 Potsdam, Germany*
[10] *University of Hertfordshire, Physics, Astronomy and Mathematics, College Lane, Hatfield AL10 9AB, United Kingdom*
[11] *INAF - Osservatorio Astronomico, Via Ranzani n. 1, 40127 Bologna, Italy*
[12] *Department of Astronomy, Columbia University, New York, NY 10027, USA*
[13] *Department of Astronomy, University of Virginia, Charlottesville, VA 22904-0818, USA*
[14] *Department of Physics and Astronomy, Iowa State University, Ames, IA, USA*
[15] *Department of Astronomy, University of Michigan, Ann Arbor, MI 48109, USA*
[16] *Warsaw University Observatory Al. Ujazdowskie 4, 00-478 Warszawa, Poland*
[17] *Departamento de Astronomia, Universidad de Concepcion, Casilla 160-C, Chile*
[18] *Department of Physics and Astronomy, Michigan State University, East Lansing, MI, USA 48824*

Accepted XXX. Received YYY; in original form ZZZ

ABSTRACT
Something something metallicity

Key words: keyword1 - keyword2 - keyword3

1 INTRODUCTION

The Carnegie RR Lyrae Program (CRRP) is a Warm *Spitzer* program (PI W. Freedman) with the aim of calibrating the mid–infrared (mid–IR) RR Lyrae period–luminosity (PL) relation. Similar to the Carnegie Hubble Program (CHP) (Freedman et al. 2011), which used mid–IR observations of Cepheids to measure the Hubble constant (H_0 Freedman et al. 2012), the results of the CRRP will be used in to provide an independent, population II calibration of the extragalactic distance scale, hence an independent measurement of H_0.

In recent years it has become increasingly important to obtain independent direct measurements of H_0. We are now in the era of precision cosmology, where the measurements of H_0 have such small uncertainties that different techniques are no longer all in agreement. For example, the results of Riess et al. (2011) and Freedman et al. (2012), both which use Cepheids and type Ia supernovae (SNe) as their base, agree very well at 74.4 ± 2.5 km s^{-1} Mpc^{-1} and 74.3 ± 2.6 km s^{-1} Mpc^{-1}. However, when we consider the latest results from *Planck*, who find 67.48 ± 0.98 km s^{-1} Mpc^{-1} (Planck Collaboration et al. 2015), there is tension. The *Planck* study derives their measurement from a model of the cosmic microwave background (CMB), so is completely independent of the Riess et al. and Freedman et al. results.

There have been several recent works that have investigated possible sources of uncertainty in the distance ladder that may contribute to the discrepancy between H_0 measurements. For example, Rigault et al. (2015) examine the differences in star formation rates

⋆ E-mail: mdurbin@stsci.edu

in type Ia SNe host galaxies. They find that the intrinsic brightness of a SNe Ia may be affected by the local host environment; i.e. whether the SN occurs in a locally star forming or locally passive environment. Efstathiou (2014) reanalysed the Cepheid data from Riess et al. (2011), and found that different outlier rejection criteria lowered the resultant value of H_0 to 70.6 ± 3.3 km s^{-1} Mpc^{-1}, making it compatible with the value from *Planck*.

The CRRP assess a systematic that was unreachable in the original CHP — the intrinsic accuracy of the mid–IR Cepheid standard candle distance scale when compared to the standard ruler distance scale of CMB and Baryon Acoustic Oscillation (BAO) measurements. With only one "test candle" it is impossible to make any assessment of this accuracy. However, when we have two standard candles with similar precision we can make meaningful comparisons and assess their systematic accuracy.

In this work we focus on the effect of metallicity on the RR Lyrae PL relation. Several Galactic Globular Clusters are being observed as part of CRRP, but ω Cen is unique in that it exhibits a measureable spread in metallicity (Freeman & Rodgers 1975; Villanova et al. 2007, 2014). **How many dex? Or how many times larger spread than a typical GGC?**

There are very few metallic or molecular transition lines in the mid–IR at typical RR Lyrae temperatures, so the effects of metallicity on luminosity should be minimised. However, ω Cen provides the ideal test bed for any effect that we may not have predicted. Such an effect is not out of the realm of possibility; for example, the CO band head at 4.5 μm has been found to have a significant dependence on metallicity, and has such prevented the IRAC 4.5 μm Cepheid observations from being used for distance measurements in the CHP. (Scowcroft et al. 2011; Monson et al. 2012; Scowcroft et al. 2015). As our concern in this program is systematic precision, we must ensure that similar effects do not plague the RRL distance scale.

In the past RR Lyrae variables have often been thought of as the poor substitute for Cepheids in terms of distance scale measurements. They are intrinsically fainter, and in the optical follow a much shallower, even horizontal, PL relation. Determining an accurate distance to an RR Lyrae (RRL) in the V band requires knowledge of its metallicity. However, in more recent years near– and mid–IR observations have shown the true power of RRL as precision distance indicators. In a similar vein to Cepheids, HST parallaxes were obtained for several Galactic RRL calibrators Benedict et al. (2011) and several groups have been studying the populations of RRL in globular clusters and nearby dwarf spheroidal galaxies (NEED REFS).

In the mid–infrared RRL exhibit similar properties to Cepheids (Madore et al. 2013). Their light curve amplitudes are minimised as we are seeing deeper into the star. At the wavelengths observed by Warm *Spitzer* (3.6 and 4.5 μm) we do not see photospheric effects, but only the effects of temperature driving the pulsation. Essentially, the mid–infrared light curve is tracing the radius change of the star. A by–product of this effect is that the intrinsic width of the RRL PL relation is also minimised in the mid–infrared (mid–IR). The PL relation for pulsational variables can be thought of as a two–dimensional projection of the three–dimensional period–luminosity–colour relation (see figure 3 of Madore & Freedman (1991) for a graphical representation). As the colour–width decreases in the mid–IR, the width of the PL naturally decreases. As one moves from the optical to the mid–IR, the slope of the PL relation steepens and its dispersion dramatically decreases; this phenomenon has been demonstrated in simulations by Catelan et al. (2004), and by several observational efforts, as illustrated in fig. 4 of Madore et al. (2013). The slope should asymptotically approach the predicted slope of the period–radius relation, resulting in a slope between −2.4 and −2.8. Through this decrease in dispersion we have found that the intrinsic width of the mid–IR PL for RRL is in fact smaller than for Cepheids – 0.05 mag compared to 0.10 mag ([**Monson et al. 2015**], (Neeley et al. 2015)). This translates to an uncertainty on an individual RR Lyrae star of 2%, compared to 4% for Cepheids.

In this work we present the mid–IR PL relation for the RRL in the ω Cen Galactic Globular Cluster (GGC). Here we present a mid–infrared of the RR Lyrae period–luminosity (PL) relation in the IRAC channels 1 and 2 centred on 3.6 and 4.5 μm respectively, as well as a preliminary investigation into metallicity effects on the PL relation.

ω Cen in particular is ideal for calibrating the RR Lyrae period–luminosity–metallicity relation, as it contains 192 known RR Lyrae (Kaluzny et al. 2004) with a metallicity range spanning over 1.5 dex (Bono 2013, priv. comm.); a metallicity spread this wide is not found in any other GGC. As noted in Sollima et al. (2006a), one of the advantages of using globular clusters to calibrate PL coefficients is that all stars in a cluster can be considered to be at the same distance from Earth. We can therefore assume that any dispersion in the PL relation is a combination of the a) the intrinsic dispersion of the PL relation, b) the photometric uncertainties, and c) dispersion induced by the spread in metallicity of the RRL. We have measured the intrinsic dispersion of the RRL PL from other clusters (e.g. M4, Neeley et al. (2015)), and our photometric uncertainties are a well defined **constraint, value?? what is the correct word?**, so the only unknown in this problem is the dispersion due to the spread in metallicity of the cluster. We are lucky with ω Cen that we can also take a second approach to establishing the metallicity effect on the RRL PL relation. As it is such a unique object, ω Cen is extremely well studied and many of its RRL have spectroscopic or photometric metallicities available. As another test of the effect of metallicity, we use these measurements to assess the γ parameter for the GGC, where

$$\gamma = \frac{\Delta \mathrm{mag}}{[Fe/H]}, \tag{1}$$

similar to γ used to quantify the effect of metallicity on the zero–point of the Cepheid PL relation.

The paper is set out as follows: Section 2 details the observations and data reduction. Section 4 describes the mid–IR PL relations and Section 5 discusses the application of these to a distance measurement of ω Cen. Section 6 and Section 7 examine the effect of metallicity on mid–IR observations of RR Lyrae variables and its implications for distance measurements and the extragalactic distance scale. In Section 8 we present our conclusions.

2 OBSERVATIONS & DATA REDUCTION

The Warm *Spitzer* observations for this work were taken as part of the Carnegie RR Lyrae Program (PI W. Freedman, PID 90002). Three fields in ω Cen were chosen; their positions and the positions of known RR Lyrae are shown in Figure 1. To obtain optimal RRL light curves we observed each field 12 times over approximately 16 hours, roughly corresponding to the period of the longest period RRL we expected in the field. The observations of all three fields were taken on 2013-05-10 and 2013-05-11. Each field was observed using *Spitzer* IRAC (Fazio et al. 2004) with a 30s frame time with a medium scale, gaussian 5–point dither pattern to mitigate any

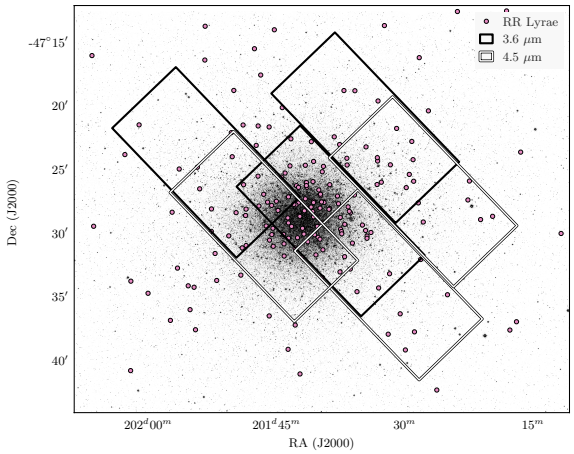

Figure 1. A K–band image of ω Cen from the FourStar camera, overlaid with the catalog of RR Lyrae (Kaluzny et al. 2004) and footprints of the three IRAC fields.

image artefacts. Images were collected in both the 3.6 and 4.5 μm channels. The elongated field shapes (seen in Figure 1) come from the design of IRAC; while the [3.6] channel is collecting on–target data, the [4.5] channel collects off target data "for free", and vice versa. We chose to include these off–target fields to maximise the number of RRL in our final sample.

The science images were created using MOPEX (Makovoz et al. 2006), first running overlap correction on the corrected BCDs (cBCDs) then mosaicking them at 0.6 arcsec pixel scale using the drizzle algorithm. Mosaicked location–correction images were created at the same time.

PSF photometry was performed using the DAOPHOT and ALLFRAME (Stetson 1987, 1994). The PSF model was created for each field/filter combination using the first epoch data. This was then applied to each other epoch. As the observations were taken so close together the effects of telescope rotation between epochs on the mosaicked PSF were minimal, so making a single good PSF model for each field/filter combination was much more efficient than creating one for every epoch.

Master star lists for ALLFRAME were created for each filter/field combination using a median mosaicked image created by MOPEX. We did not use the same single master star list for both filters as only a small proportion (1/3) of the 3.6 μm and 4.5 μm fields overlap each other. Instead we performed separate ALLFRAME reductions for each filter, and combined the results after the fact using DAOMATCH and DAOMASTER. Our photometry is calibrated to the standard system set by Reach et al. (2005).

The primary limiting factor in this data is crowding: 77 RR Lyrae variables out of the original catalog of 192 (Kaluzny et al. 2004) were rejected due to crowding. To decide which stars to reject we compared the *Spitzer* images to a K–band image from the FourStar infrared camera on Magellan (Persson et al. 2013), with a resolution of 0.159 arcsec. This enabled us to see which stars were significantly contaminated and adjust our final sample accordingly.

3 RESULTS

Our final photometry catalog, including magnitudes and errors for JHK, 3.6 μm, and 4.5 μm is presented in Table 1.

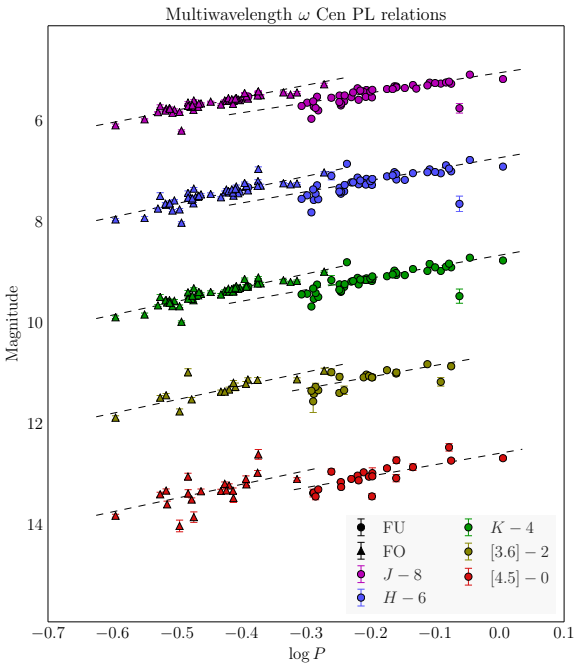

Figure 2. PL relations for JHK, 3.6 μm, and 4.5 μm photometry assuming an [Fe/H]= −1.584, corresponding to the average photometric metallicity from Rey et al. (2000). All uncrowded RRL for which we have photometry are included in these fits.

The average magnitudes are calculated by first converting the individual values into fluxes, then taking the mean value. The photometric errors of the time series data are added in quadrature and divided by the square root of the total number of observations to obtain the final error value.

4 PERIOD–LUMINOSITY RELATIONS

Our full, uncrowded RR Lyrae sample consists of 96 stars in J and H, 98 in K, 36 in 3.6 μm, and 43 in 4.5 μm. The PL fits to this sample are shown in Figure 2, and the distance moduli and reddening values obtained from these fits are shown in Figure **get correct plot for thisÑgot overwritten with wrong data**.

For the final PL relations, we use only the stars for which we have photometry in all five bandpasses. Our final RRL sample consists of 25 RRL (12 fundamental mode and 13 first overtone). While this final sample is sparse, it reduces sampling bias by ensuring that the same range of periods and metallicities are sampled for each wavelength. We do not need to be concerned that cutting the sample introduces other types of bias. As previously mentioned, the intrinsic PL width of RR Lyrae variables in the mid–IR is half that of Cepheids (0.05 mag vs. 0.10 mag); based on the scatter of the PL residuals, the cut samples encompass the full width at all wavelengths. Similarly, the ratio of ω Cen's diameter to its distance is approximately 1% (**wikipedia'd, will find ref if needed**), so we can make the simplifying assumption that all the RRL are at the same distance and thus do not need to concern ourselves with sampling a range of distances.

We use the near– and mid–infrared PL relation parameters presented in **VS CHECK REF FOR BRAGA PAPER** as fiducial in all of our PL fitting. With the use of the theoretical PL relation

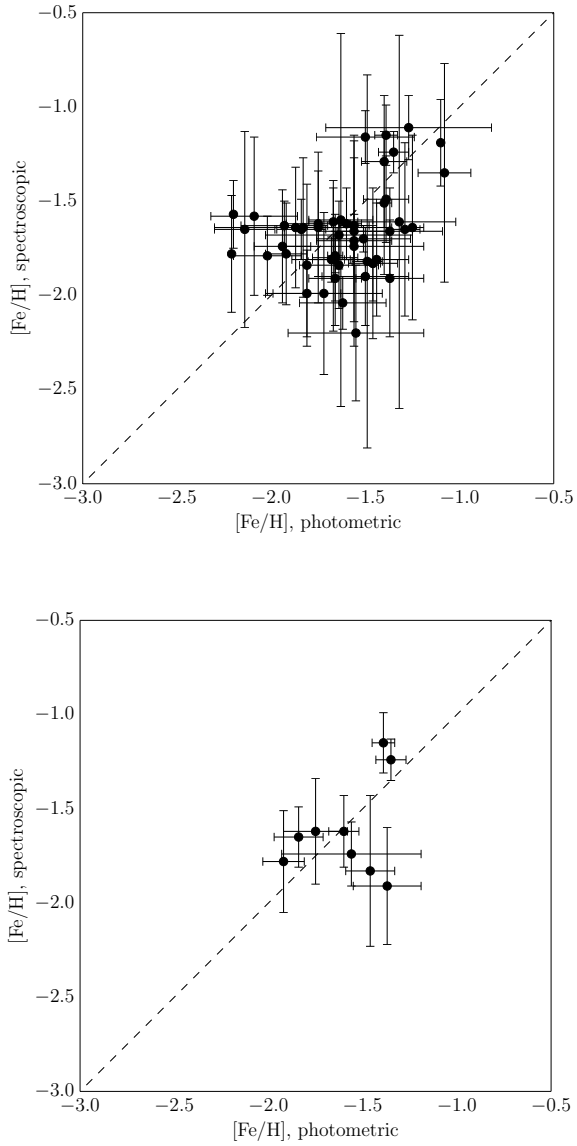

Figure 3. Spectroscopic vs. photometric measurements of [Fe/H] for RR Lyrae variables in ω Cen. Top: All stars for which both catalogs have [Fe/H] measurements. Bottom: only the stars which appear in our final sample.

coefficients, the distance modulus becomes the only free parameter in our fit. We fit all distance moduli using a weighted least–squares method, and fit the distance modulus to each pulsation mode in each wavelength separately.

Not all stars in our sample have known metallicity values, so we use an average [Fe/H] value for all RR Lyrae variables in the cluster. We use both photometric (Rey et al. 2000) and spectroscopic (Sollima et al. 2006b) metallicities for comparison. We find that there is little correspondence between individual metallicity measurements for stars which have both spectroscopic and photometric metallicity values, as shown in Figure 3, and that the average metallicities of the spectroscopic and photometric catalogs differ by nearly 0.1 dex. We use a mean photometric [Fe/H] of −1.584 and a spectroscopic [Fe/H] of −1.677.

The RRL PL relations for each adopted average metallicity are

Table 1. Mid–IR RR Lyrae period–luminosity relations for ω Cen [REF]. **The σ parameter here is from the draft I was sent, I assume it's the scatter? Don't know for sure though**

Band	Mode	[Fe/H]	a	b	c	σ
[3.6]	FO	−1.584	−1.344	−2.718	0.152	0.021
	FO	−1.677	−1.344	−2.718	0.152	0.021
	FU	−1.584	−0.786	−2.276	0.184	0.035
	FU	−1.677	−0.786	−2.276	0.184	0.035
[4.5]	FO	−1.584	−1.348	−2.720	0.153	0.021
	FO	−1.677	−1.348	−2.720	0.153	0.021
	FU	−1.584	−0.775	−2.262	0.190	0.036
	FU	−1.677	−0.775	−2.262	0.190	0.036

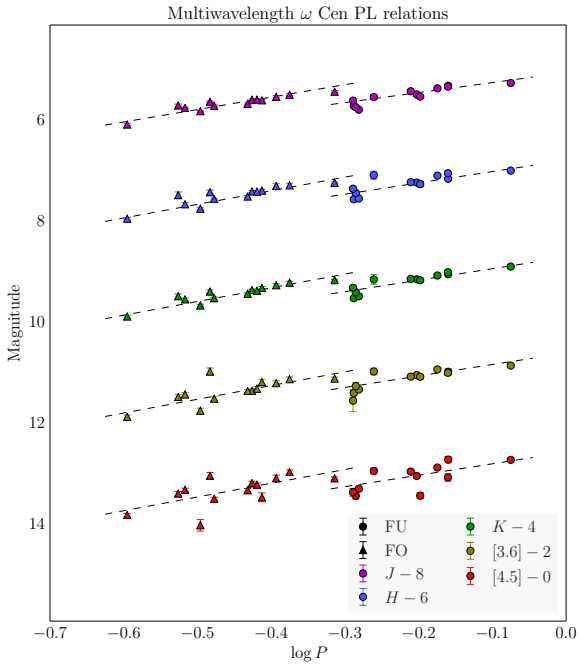

Figure 4. PL relations for JHK, 3.6 μm, and 4.5 μm photometry assuming an [Fe/H]= −1.584, corresponding to the average photometric metallicity from Rey et al. (2000). Only those RRL that appear in all five near– and mid–infrared bands are included in the fit.

shown in Figures 5 and 4 and described in Table 1. The relations take the form

$$M = a + b \times \log P + c \times [Fe/H] \quad (2)$$

where a, b, and c are theoretically derived coefficients.

5 DISTANCE MODULI

We combine the uncorrected distance moduli from each bandpass to obtain a mean reddening–corrected distance modulus. We fit the near–infrared reddening law from Cardelli et al. (1989) and mid–infrared law from Indebetouw et al. (2005) simultaneously, assuming the ratio of total to selective absorption $R_V = 3.1$. The resulting fits are shown in Figures 6 and 7.

Using photometric metallicities we obtain a mean reddening–corrected distance modulus of $\mu_0 = 13.678 \pm 0.053$, and with

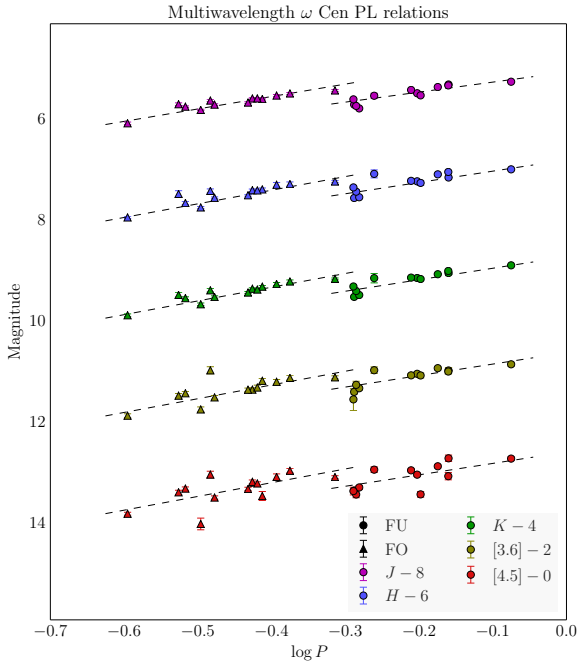

Figure 5. PL relations for *JHK*, 3.6 μm, and 4.5 μm photometry assuming an [Fe/H]= −1.677, corresponding to the average spectroscopic metallicity from Sollima et al. (2006b). Only those RRL that appear in all five near– and mid–infrared bands are included in the fit.

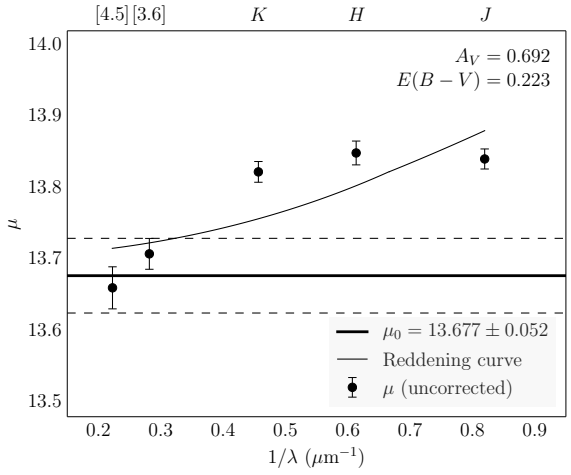

Figure 6. Distance moduli for *JHK*, 3.6 μm, and 4.5 μm photometry using the average photometric metallicity from Rey et al. (2000)

spectroscopic metallicities we obtain $\mu_0 = 13.694 \pm 0.053$. The difference between the two distance moduli is less than 0.02 mag, well within the ±0.053 mag errors. The fact that the two distance moduli are indistinguishable is the first indication that the infrared RRL PL relations are not sensitive to metallicity effects.

We average these distance moduli (thus essentially averaging the metallicities as well) to find a true mean distance modulus of $\mu_0 = 13.686 \pm 0.053$, which is in excellent agreement with prior measurements using near–infrared RR Lyrae period–luminosity relations (Del Principe et al. 2006) and and the eclipsing binary

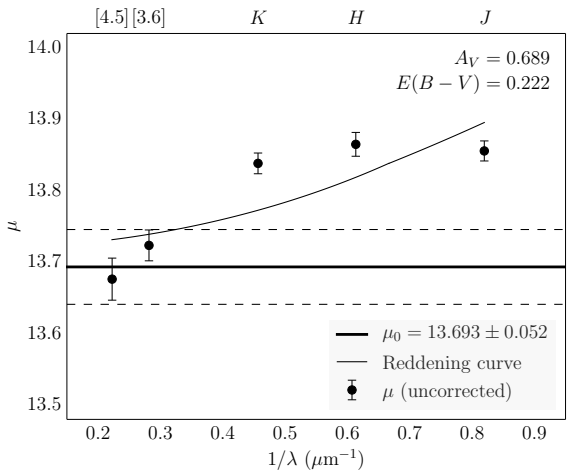

Figure 7. Distance moduli for *JHK*, 3.6 μm, and 4.5 μm photometry using the average spectroscopic metallicity from Sollima et al. (2006b)

OGLEGC17 (Thompson et al. 2001), but significantly higher than the distances measured by dynamical modelling (van de Ven et al. 2006; Watkins et al. 2013)

6 METALLICITY

Theoretical models suggest that the metallicity dependence of the RR Lyrae PL relation should decrease monotonically from the optical to the near-infrared (Catelan et al. 2004; Bono et al. 2001), and observational evidence corroborates this; previous investigations performed on WISE data suggest no obvious metallicity dependence in the mid-IR PL relations (Madore et al. 2013). In the case of Cepheids, Scowcroft et al. (2011) and Scowcroft et al. (2015) have shown that in the 4.5 μm bandpass there is absorption due to a CO bandhead at 4.65 μm, which strengthens the metallicity dependence of the PL relation in this bandpass. However, this effect is due to the low temperature of Cepheid atmospheres and disappears in the hottest, shortest-period Cepheids, as the CO dissociates at temperatures above 6000 K (Monson et al. 2012). As even the coolest RRL have temperatures over 6000 K [**ref?**], we expect to see no such CO absorption in the 4.5 μm PL relation. However, there may be other unanticipated metallicity effects in the mid-IR PL relations. If there are any such effects, they must be smaller than the dispersion of the PL relations themselves.

If there is any correlation between [Fe/H] and the PL residuals, we expect it to be a linear one, consistent with the theoretical metallicity terms in the PL relation, $c \times [Fe/H]$. We fit a relation of the form

$$\Delta\text{mag} = \gamma \times [Fe/H] + d \quad (3)$$

to the 3.6 μm and 4.5 μm PL residuals and metallicity values for stars with known individual metallicity values, as shown in Figures 12, 9, 13, and 11. We find that although the scatter in the 3.6 μm and 4.5 μm PL relations is higher for ω Cen than it is for M4 (Neeley et al. 2015) **can't find Inno+ 2014 ref**, there is no evidence that it is due to metallicity. When we examine [Fe/H] vs. Δ3.6 μm and Δ4.5 μm, γ is within 2σ of zero for all fits, indicating that there is no significant metallicity dependence in the PL residuals. When the outlier in [Fe/H] vs. 3.6 μm at [Fe/H] = −2.0 is removed from

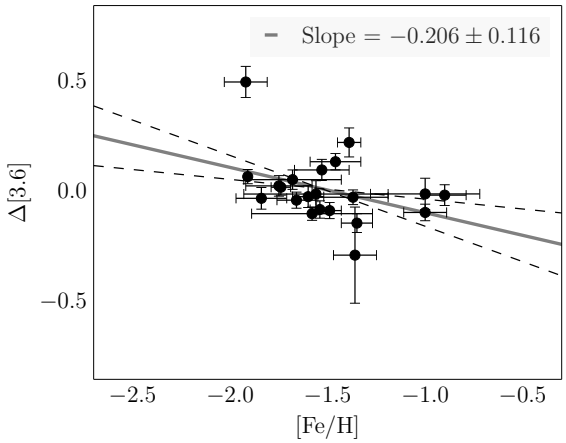

Figure 8. [Fe/H] vs. Δ3.6 μm using photometric metallicities

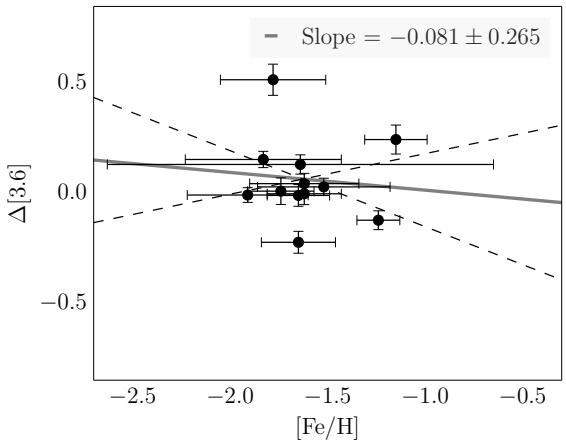

Figure 9. [Fe/H] vs. Δ3.6 μm using spectroscopic metallicities

the photometric metallicities, the slopes of [Fe/H] vs. 3.6 μm and 4.5 μm both move within 1σ of zero.

7 DISCUSSION

This section we can work on once you've worked on the others. I think it will write a lot of itself after you've done the other bits.

Alternative explanations for the increased scatter relative to M4 include crowding and [other things here].

8 CONCLUSIONS

ACKNOWLEDGEMENTS

We thank Eric Persson for his many contributions to this project.

This work is based on observations made with the Spitzer Space Telescope, which is operated by the Jet Propulsion Laboratory, California Institute of Technology under a contract with NASA. Support for this work was provided by NASA through an award issued by JPL/Caltech.

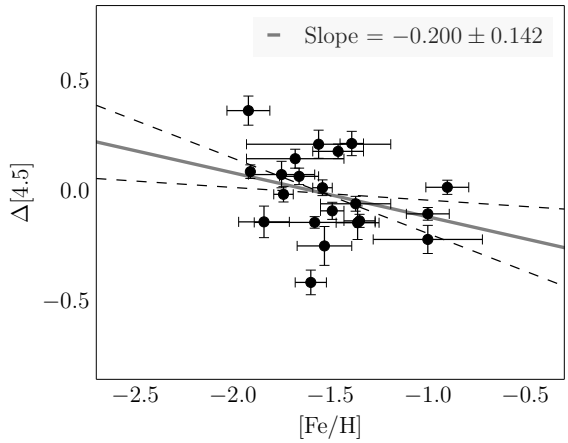

Figure 10. [Fe/H] vs. Δ4.5 μm using photometric metallicities

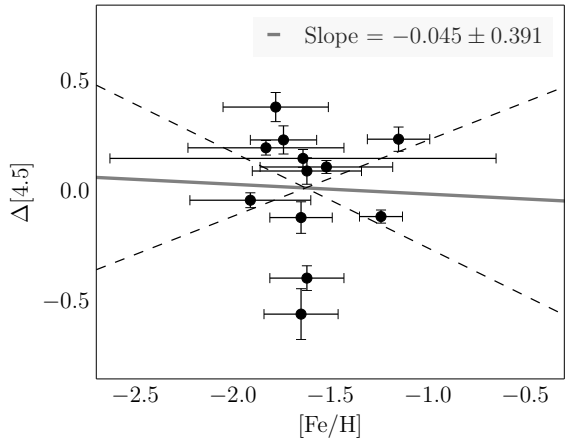

Figure 11. [Fe/H] vs. Δ4.5 μm using spectroscopic metallicities

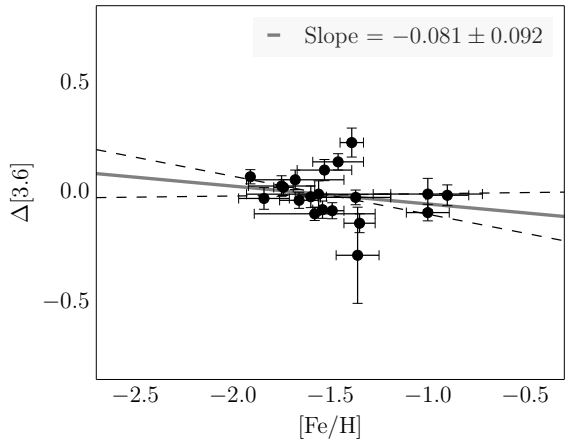

Figure 12. [Fe/H] vs. Δ3.6 μm using photometric metallicities, with outliers removed

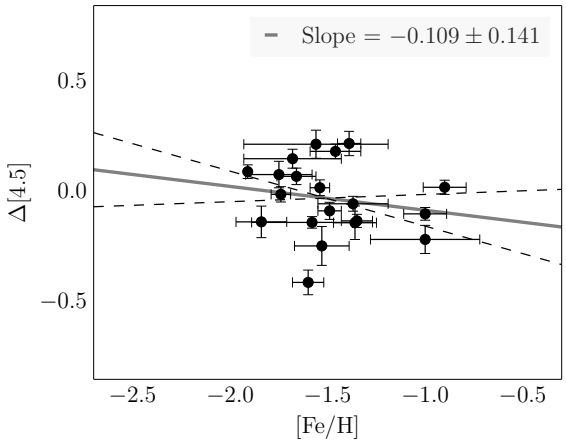

Figure 13. [Fe/H] vs. Δ4.5 μm using photometric metallicities, with outliers removed

REFERENCES

Benedict G. F., et al., 2011, AJ, 142, 187
Bono G., Caputo F., Castellani V., Marconi M., Storm J., 2001, MNRAS, 326, 1183
Cardelli J. A., Clayton G. C., Mathis J. S., 1989, ApJ, 345, 245
Catelan M., Pritzl B. J., Smith H. A., 2004, ApJS, 154, 633
Del Principe M., et al., 2006, ApJ, 652, 362
Efstathiou G., 2014, MNRAS, 440, 1138
Fazio G. G., et al., 2004, ApJS, 154, 10
Freedman W. L., et al., 2011, AJ, 142, 192
Freedman W. L., Madore B. F., Scowcroft V., Burns C., Monson A., Persson S. E., Seibert M., Rigby J., 2012, ApJ, 758, 24
Freeman K. C., Rodgers A. W., 1975, ApJ, 201, L71
Indebetouw R., et al., 2005, ApJ, 619, 931
Kaluzny J., Olech A., Thompson I. B., Pych W., Krzemiński W., Schwarzenberg-Czerny A., 2004, A&A, 424, 1101
Madore B. F., Freedman W. L., 1991, PASP, 103, 933
Madore B. F., et al., 2013, ApJ, 776, 135
Makovoz D., Roby T., Khan I., Booth H., 2006, in Society of Photo-Optical Instrumentation Engineers (SPIE) Conference Series. p. 0, doi:10.1117/12.672536
Monson A. J., Freedman W. L., Madore B. F., Persson S. E., Scowcroft V., Seibert M., Rigby J. R., 2012, ApJ, 759, 146
Neeley J. R., et al., 2015, preprint, (arXiv:1505.07858)
Persson S. E., et al., 2013, PASP, 125, 654
Planck Collaboration et al., 2015, preprint, (arXiv:1502.01589)
Reach W. T., et al., 2005, PASP, 117, 978
Rey S.-C., Lee Y.-W., Joo J.-M., Walker A., Baird S., 2000, AJ, 119, 1824
Riess A. G., et al., 2011, ApJ, 730, 119
Rigault M., et al., 2015, ApJ, 802, 20
Scowcroft V., Freedman W. L., Madore B. F., Monson A. J., Persson S. E., Seibert M., Rigby J. R., Sturch L., 2011, ApJ, 743, 76
Scowcroft V., Freedman W. L., Madore B. F., Monson A., Persson S. E., Rich J., Seibert M., Rigby J. R., 2015, preprint, (arXiv:1502.06995)
Sollima A., Cacciari C., Valenti E., 2006a, MNRAS, 372, 1675
Sollima A., Borissova J., Catelan M., Smith H. A., Minniti D., Cacciari C., Ferraro F. R., 2006b, ApJ, 640, L43
Stetson P. B., 1987, PASP, 99, 191
Stetson P. B., 1994, PASP, 106, 250
Thompson I. B., Kaluzny J., Pych W., Burley G., Krzeminski W., Paczyński B., Persson S. E., Preston G. W., 2001, AJ, 121, 3089
Villanova S., et al., 2007, ApJ, 663, 296
Villanova S., Geisler D., Gratton R. G., Cassisi S., 2014, ApJ, 791, 107
Watkins L. L., van de Ven G., den Brok M., van den Bosch R. C. E., 2013, MNRAS, 436, 2598
van de Ven G., van den Bosch R. C. E., Verolme E. K., de Zeeuw P. T., 2006, A&A, 445, 513

Table 1: JHK, 3.6 μm, and 4.5 μm photometry of the RR Lyrae variables in ω Cen

ID	RA (J2000)	Dec (J2000)	J	σ_J	H	σ_H	K	σ_K	[3.6]	$\sigma_{[3.6]}$	[4.5]	$\sigma_{[4.5]}$	P (days)	Mode	[Fe/H], p	$\sigma_{[Fe/H]}$, p	[Fe/H], s	$\sigma_{[Fe/H]}$, s
3	13:25:56.15	-47:25:53.8	13.247	0.017	12.982	0.018	12.882	0.017	12.841	0.039	12.708	0.036	0.841	0	-1.54	0.05	–	–
4	13:26:12.93	-47:24:18.8	13.475	0.016	13.219	0.021	13.133	0.020	13.030	0.036	13.026	0.035	0.627	0	-1.74	0.05	–	–
5	13:26:18.33	-47:23:12.4	13.700	0.017	13.549	0.020	13.507	0.027	13.387	0.043	13.340	0.030	0.515	0	-1.35	0.08	-1.24	0.11
7	13:27:00.90	-47:14:00.5	13.333	0.009	13.151	0.031	13.036	0.018	–	–	–	–	0.713	0	-1.46	0.08	–	–
8	13:27:48.45	-47:28:20.3	13.505	0.015	13.258	0.016	13.223	0.014	–	–	–	–	0.521	0	-1.91	0.28	–	–
9	13:25:59.58	-47:26:24.0	13.776	0.017	13.534	0.021	13.470	0.016	13.315	0.036	13.279	0.039	0.523	0	-1.49	0.06	–	–
10	13:26:06.99	-47:24:36.6	13.579	0.014	13.395	0.023	13.345	0.019	13.342	0.037	13.168	0.037	0.375	1	-1.66	0.10	–	–
11	13:26:30.59	-47:23:01.6	13.481	0.014	13.307	0.028	13.219	0.025	13.050	0.058	–	–	0.565	0	-1.67	0.13	-1.61	0.22
12	13:26:27.21	-47:24:06.2	13.590	0.018	13.379	0.028	13.305	0.025	13.168	0.048	13.448	0.088	0.387	1	-1.53	0.14	–	–
13	13:25:58.18	-47:25:21.6	13.353	0.019	13.081	0.022	13.058	0.017	12.918	0.032	12.860	0.031	0.669	0	-1.91	0.000	–	–
14	13:25:59.74	-47:39:09.6	13.588	0.011	13.343	0.020	13.365	0.016	–	–	13.299	0.045	0.377	1	-1.71	0.13	–	–
15	13:26:27.11	-47:24:38.0	13.245	0.018	13.020	0.031	12.954	0.025	13.149	0.084	–	–	0.811	0	-1.64	0.39	-1.68	0.18
16	13:27:37.69	-47:37:34.8	13.680	0.015	13.502	0.022	13.437	0.018	–	–	–	–	0.330	1	-1.29	0.08	-1.65	0.46
18	13:27:45.11	-47:24:56.6	13.371	0.010	13.131	0.024	13.100	0.016	13.006	0.043	–	–	0.622	0	-1.78	0.28	–	–
20	13:27:14.05	-47:28:06.3	13.410	0.015	13.210	0.036	13.125	0.025	13.060	0.039	12.940	0.029	0.616	0	–	–	-1.52	0.34
21	13:26:11.17	-47:25:58.8	13.578	0.016	13.399	0.027	13.361	0.020	13.301	0.047	13.200	0.032	0.381	1	-0.90	0.11	–	–
22	13:27:41.04	-47:34:07.6	13.572	0.012	13.380	0.016	13.288	0.017	–	–	–	–	0.396	1	-1.63	0.17	-1.60	0.99
23	13:26:46.50	-47:24:39.5	13.941	0.025	13.794	0.048	13.658	0.033	13.325	0.064	–	–	0.511	0	-1.08	0.14	-1.35	0.58
24	13:27:38.32	-47:34:14.5	13.419	0.012	13.218	0.014	13.138	0.014	–	–	–	–	0.462	1	-1.86	0.03	–	–
30	13:26:15.94	-47:29:56.0	13.521	0.021	13.287	0.046	13.251	0.030	13.188	0.047	13.071	0.060	0.404	1	-1.75	0.17	-1.62	0.28
32	13:27:03.32	-47:21:38.9	13.508	0.009	13.244	0.018	13.132	0.018	–	–	–	–	0.620	0	-1.53	0.16	–	–
33	13:25:51.60	-47:29:05.8	13.338	0.015	13.106	0.022	13.091	0.019	–	–	13.006	0.035	0.602	0	-2.09	0.23	-1.58	0.42
34	13:26:07.21	-47:33:10.4	13.273	0.014	13.018	0.014	12.916	0.013	–	–	12.838	0.065	0.734	0	-1.71	0.000	–	–
35	13:26:53.21	-47:22:34.7	13.586	0.012	13.463	0.024	13.356	0.023	–	–	–	–	0.387	1	-1.56	0.08	-1.63	0.36
36	13:27:10.11	-47:15:29.8	13.534	0.007	13.372	0.019	13.307	0.014	–	–	–	–	0.380	1	-1.49	0.23	–	–
38	13:27:03.30	-47:36:30.2	13.226	0.015	12.943	0.019	12.814	0.018	–	–	–	–	0.779	0	-1.75	0.18	-1.64	0.40
39	13:27:59.77	-47:34:42.3	13.560	0.009	13.415	0.014	13.308	0.014	–	–	–	–	0.393	1	-1.96	0.29	–	–
40	13:26:24.56	-47:30:46.2	13.517	0.022	13.250	0.051	13.153	0.033	13.062	0.049	13.416	0.056	0.634	0	-1.60	0.08	-1.62	0.19
44	13:26:22.39	-47:34:35.3	13.677	0.014	13.425	0.023	13.368	0.018	–	–	13.132	0.036	0.568	0	-1.40	0.12	-1.29	0.35
45	13:25:30.88	-47:27:21.0	13.513	0.015	13.201	0.015	13.164	0.014	–	–	13.070	0.028	0.589	0	-1.78	0.25	–	–
46	13:25:30.23	-47:25:51.8	13.299	0.016	12.998	0.017	12.947	0.014	–	–	–	–	0.687	0	-1.88	0.17	–	–
47	13:25:56.46	-47:24:12.0	13.420	0.020	13.223	0.018	13.150	0.018	13.099	0.030	13.073	0.026	0.485	1	-1.58	0.31	–	–
49	13:26:07.78	-47:37:55.5	13.566	0.012	13.238	0.019	13.220	0.016	–	–	13.099	0.049	0.605	0	-1.98	0.11	–	–
50	13:25:53.94	-47:27:35.8	13.647	0.014	13.402	0.015	13.362	0.014	–	–	13.305	0.056	0.386	1	-1.59	0.19	–	–
51	13:26:42.66	-47:24:21.4	13.597	0.014	13.378	0.033	13.270	0.029	13.315	0.083	–	–	0.574	0	-1.64	0.21	-1.84	0.23
54	13:26:23.54	-47:18:47.7	13.281	0.016	12.998	0.017	12.954	0.015	12.799	0.030	–	–	0.773	0	-1.66	0.12	-1.80	0.23
56	13:25:55.53	-47:37:44.1	13.643	0.009	13.386	0.022	13.353	0.017	–	–	13.232	0.035	0.568	0	-1.26	0.15	–	–
57	13:27:49.38	-47:36:50.5	13.234	0.015	12.995	0.018	12.882	0.014	–	–	–	–	0.794	0	-1.89	0.14	–	–
58	13:26:13.05	-47:24:03.0	13.660	0.017	13.495	0.018	13.421	0.021	13.345	0.033	13.309	0.034	0.370	1	-1.37	0.18	-1.91	0.31
59	13:26:18.43	-47:29:46.7	13.727	0.023	13.424	0.043	13.391	0.033	13.248	0.071	13.418	0.064	0.519	0	-1.00	0.28	–	–
63	13:25:07.96	-47:36:54.1	13.223	0.017	12.862	0.017	12.869	0.012	–	–	–	–	0.826	0	-1.73	0.09	–	–
64	13:26:02.22	-47:36:19.2	13.638	0.013	13.438	0.022	13.407	0.022	–	–	13.314	0.044	0.344	1	-1.46	0.23	–	–
66	13:26:33.08	-47:22:25.2	13.542	0.011	13.359	0.022	13.264	0.020	13.103	0.035	–	–	0.407	1	-1.68	0.34	–	–
67	13:26:28.62	-47:18:46.9	13.610	0.014	13.384	0.016	13.326	0.015	13.368	0.047	–	–	0.564	0	-1.10	0.000	-1.19	0.23
68	13:26:12.80	-47:19:35.7	13.258	0.021	13.004	0.015	12.970	0.015	12.928	0.050	–	–	0.535	1	-1.60	0.01	–	–
69	13:25:11.02	-47:37:33.5	–	–	–	–	13.112	0.014	–	–	–	–	0.635	0	-1.52	0.14	–	–
70	13:27:27.76	-47:33:42.7	13.529	0.013	13.282	0.029	13.254	0.022	–	–	–	–	0.391	1	-1.94	0.15	-1.74	0.30
72	13:27:33.11	-47:16:22.9	13.554	0.010	13.339	0.017	13.311	0.014	–	–	–	–	0.385	1	-1.32	0.22	–	–
73	13:25:53.75	-47:16:10.8	13.480	0.018	13.251	0.017	13.215	0.016	–	–	–	–	0.575	0	-1.50	0.09	–	–
74	13:27:07.22	-47:17:33.9	13.622	0.008	13.457	0.016	13.405	0.015	–	–	–	–	0.503	0	-1.83	0.36	–	–
75	13:27:19.70	-47:18:46.5	13.410	0.011	13.175	0.028	13.137	0.025	–	–	–	–	0.422	1	-1.49	0.08	-1.82	0.99
76	13:26:57.23	-47:20:07.7	13.634	0.012	13.488	0.017	13.449	0.020	–	–	–	–	0.338	1	-1.45	0.13	–	–
77	13:27:20.89	-47:22:05.6	13.474	0.013	13.264	0.028	13.199	0.021	–	–	–	–	0.426	1	-1.81	0.000	-1.84	0.43
79	13:28:24.99	-47:29:25.2	13.382	0.010	13.162	0.016	13.123	0.015	–	–	–	–	0.608	0	-1.39	0.18	–	–
81	13:27:36.68	-47:24:48.3	13.542	0.012	13.326	0.033	13.286	0.025	13.248	0.076	–	–	0.389	1	-1.72	0.31	-1.99	0.43
82	13:27:35.61	-47:26:30.3	13.579	0.016	13.324	0.024	13.296	0.018	–	–	13.827	0.104	0.336	1	-1.56	0.20	-1.71	0.56
83	13:27:08.42	-47:21:34.1	13.603	0.010	13.431	0.024	13.370	0.022	–	–	–	–	0.357	1	-1.30	0.22	–	–
84	13:24:47.45	-47:29:56.5	–	–	12.833	0.017	12.781	0.016	–	–	–	–	0.580	0	-1.47	0.10	–	–
85	13:25:06.49	-47:23:34.0	13.344	0.011	–	–	–	–	–	–	–	–	0.743	0	-1.87	0.31	–	–

Continued on next page

Table 1 – *Continued from previous page*

ID	RA (J2000)	Dec (J2000)	J	σ_J	H	σ_H	K	σ_K	[3.6]	$\sigma_{[3.6]}$	[4.5]	$\sigma_{[4.5]}$	P (days)	Mode	[Fe/H], p	$\sigma_{[Fe/H]}$, p	[Fe/H], s	$\sigma_{[Fe/H]}$, s
94	13:25:57.06	-47:22:46.1	14.070	0.024	13.934	0.022	13.870	0.027	13.858	0.038	13.799	0.029	0.254	1	-1.00	0.11	–	–
95	13:25:24.95	-47:28:53.2	13.497	0.015	13.269	0.017	13.264	0.017	–	–	13.178	0.024	0.405	1	-1.84	0.55	–	–
97	13:27:08.49	-47:25:30.9	13.302	0.010	13.143	0.029	13.034	0.022	12.964	0.061	12.702	0.064	0.692	0	-1.56	0.37	-1.74	0.17
101	13:27:30.24	-47:29:51.0	13.708	0.016	13.484	0.030	13.436	0.023	–	–	–	–	0.341	1	-1.88	0.32	–	–
102	13:27:22.11	-47:30:12.3	13.320	0.012	13.033	0.022	12.993	0.020	12.984	0.049	13.056	0.072	0.691	0	-1.84	0.13	-1.65	0.16
103	13:27:14.29	-47:28:36.3	13.620	0.018	13.409	0.040	13.377	0.034	12.960	0.071	13.024	0.066	0.329	1	-1.92	0.11	-1.78	0.27
104	13:28:07.76	-47:33:44.9	13.732	0.096	13.626	0.154	13.452	0.141	–	–	–	–	0.867	0	-1.83	0.18	–	–
105	13:27:46.02	-47:32:43.9	13.768	0.014	13.615	0.020	13.533	0.018	–	–	–	–	0.335	1	-1.24	0.18	–	–
107	13:27:14.05	-47:30:57.9	13.597	0.017	13.340	0.038	13.301	0.030	13.535	0.219	13.351	0.076	0.514	0	-1.36	0.11	–	–
115	13:26:12.30	-47:34:17.5	13.401	0.012	13.176	0.017	13.103	0.013	–	–	–	–	0.630	0	-1.87	0.01	-1.64	0.32
117	13:26:19.91	-47:29:21.0	13.480	0.020	13.274	0.043	13.202	0.031	13.110	0.044	12.949	0.043	0.422	1	-1.68	0.25	–	–
120	13:26:25.52	-47:32:48.6	13.525	0.049	13.072	0.079	13.135	0.094	12.958	0.066	12.927	0.055	0.549	0	-1.39	0.06	-1.15	0.16
121	13:26:28.17	-47:31:50.5	13.741	0.016	13.648	0.033	13.531	0.026	13.414	0.037	13.302	0.033	0.304	1	-1.46	0.13	-1.83	0.40
122	13:26:30.31	-47:33:02.2	13.369	0.018	13.132	0.042	13.062	0.024	13.057	0.052	13.019	0.043	0.635	0	-2.02	0.18	-1.79	0.21
123	13:26:51.17	-47:37:13.2	13.462	0.016	13.239	0.019	13.174	0.017	–	–	–	–	0.474	1	-1.64	0.01	–	–
124	13:26:54.49	-47:39:07.5	13.708	0.013	13.510	0.018	13.482	0.023	–	–	–	–	0.332	1	-1.33	0.23	–	–
125	13:26:48.92	-47:41:03.7	13.420	0.015	13.200	0.016	13.153	0.015	–	–	–	–	0.593	0	-1.67	0.22	-1.81	0.38
126	13:28:08.03	-47:40:46.7	13.642	0.011	13.467	0.017	13.370	0.016	–	–	–	–	0.342	1	-1.31	0.13	–	–
127	13:25:19.36	-47:28:37.6	–	–	–	–	13.579	0.018	–	–	13.573	0.063	0.305	1	-1.59	0.08	–	–
128	13:26:17.75	-47:30:13.0	13.207	0.018	12.927	0.032	12.810	0.020	–	–	12.445	0.074	0.835	0	-1.88	0.04	–	–
130	13:26:09.93	-47:13:40.0	13.688	0.021	13.527	0.032	13.418	0.025	–	–	–	–	0.493	0	-1.46	0.17	–	–
147	13:27:15.86	-47:31:09.2	13.397	0.012	12.934	0.041	13.083	0.022	–	–	12.585	0.096	0.423	1	-1.66	0.14	–	–
149	13:27:32.94	-47:13:43.6	13.354	0.015	13.061	0.035	13.024	0.024	–	–	–	–	0.683	0	-1.21	0.24	–	–
150	13:27:40.21	-47:36:00.1	13.068	0.019	12.757	0.025	12.692	0.018	–	–	–	–	0.899	0	-1.76	0.34	–	–
151	13:28:25.40	-47:16:00.2	13.501	0.013	13.301	0.020	13.265	0.016	–	–	–	–	0.408	0	-1.30	0.24	–	–
163	13:25:49.42	-47:20:21.5	13.763	0.019	13.557	0.016	13.545	0.025	–	–	–	–	0.313	1	-1.18	0.27	–	–
168	13:25:52.78	-47:32:02.9	14.176	0.015	14.000	0.020	13.960	0.018	–	–	–	–	0.321	1	–	–	–	–
169	13:27:20.47	-47:23:59.1	13.805	0.013	13.735	0.019	13.652	0.025	13.734	0.050	14.001	0.116	0.319	1	–	–	-1.65	0.19
184	13:27:28.50	-47:31:35.4	13.778	0.012	13.624	0.028	13.536	0.019	–	–	–	–	0.303	1	–	–	–	–
185	13:26:04.13	-47:21:45.0	13.701	0.016	13.545	0.018	13.508	0.023	13.496	0.036	13.479	0.033	0.333	1	–	–	–	–
261	13:27:15.41	-47:21:29.5	13.431	0.009	13.212	0.019	13.113	0.020	–	–	–	–	0.403	1	–	–	-1.50	0.35
263	13:26:13.13	-47:26:09.7	13.155	0.017	12.888	0.017	12.746	0.016	–	–	12.660	0.034	1.012	0	–	–	-1.73	0.19
274	13:26:43.73	-47:22:48.2	13.828	0.011	13.758	0.023	13.650	0.022	–	–	–	–	0.311	1	–	–	–	–
276	13:27:16.51	-47:33:17.6	13.727	0.021	13.614	0.046	13.533	0.024	–	–	–	–	0.308	1	–	–	–	–
280	13:27:09.33	-47:23:05.7	13.951	0.012	13.905	0.026	13.816	0.029	–	–	–	–	0.282	1	–	–	–	–
285	13:25:40.20	-47:34:48.4	13.687	0.017	13.504	0.027	13.503	0.015	–	–	13.358	0.074	0.329	1	–	–	–	–
288	13:28:10.32	-47:23:47.8	13.809	0.011	13.719	0.016	13.635	0.019	–	–	–	–	0.295	1	–	–	–	–
289	13:28:03.68	-47:21:27.9	13.743	0.013	13.618	0.015	13.584	0.022	–	–	–	–	0.308	1	–	–	–	–
291	13:26:38.52	-47:33:28.0	13.674	0.018	13.518	0.044	13.444	0.026	–	–	–	–	0.334	1	–	–	–	–
357	13:26:17.77	-47:30:23.4	13.692	0.027	13.468	0.064	13.468	0.045	13.462	0.044	13.375	0.041	0.298	1	–	–	-1.64	0.99

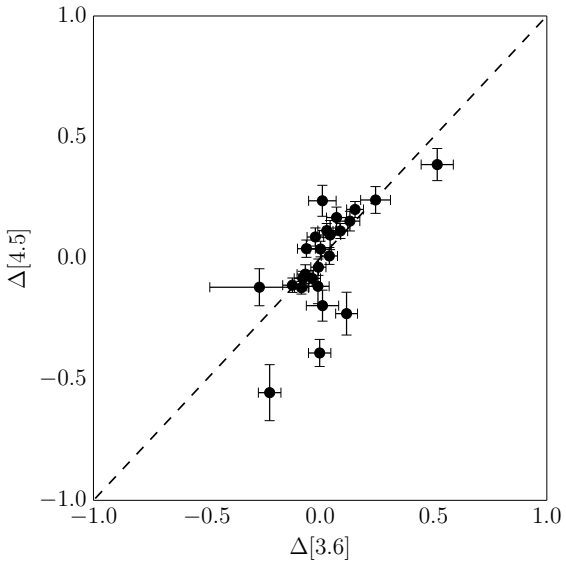

Figure 1. Δ3.6 μm vs. Δ4.5 μm using spectroscopic metallicities

This paper has been typeset from a TEX/LATEX file prepared by the author.

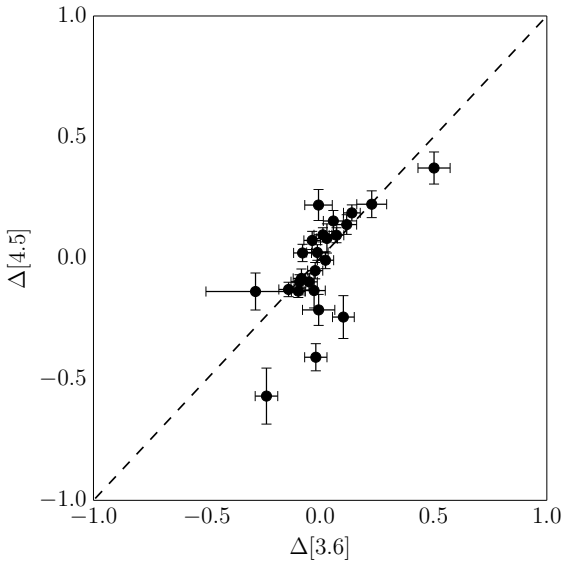

Figure 2. Δ3.6 μm vs. Δ4.5 μm using photometric metallicities